Lamb Waves Boundary Reflections in an Aluminium Plate for Defect Detection related to Structural Health Monitoring.

Aurelia MULLER [1], Bradley ROBERTSON-WELSH [2], Patrick GAYDECKI [3], Matthieu GRESIL[4], Constantinos SOUTIS [1]

[1] Aerospace Research Institute, University of Manchester, Sackville Street, Manchester. M139PL, UK.
Aurelia.Muller@postgrad.manchester.ac.uk

[2] School of Mechanical, Aerospace and Civil Engineering, University of Manchester, Sackville Street, Manchester, M139PL, UK.
Bradley.Robertsonwelsh@manchester.ac.uk

[3] School of Electrical and Electronic Engineering, University of Manchester, Sackville Street, Manchester, M139PL, UK.

[4] i-Composites lab, School of Materials, University of Manchester, Sackville Street, Manchester, M139PL, UK.

Key words: Lamb waves, reflection, signal processing.

Abstract

The aim of this investigation is to develop a post-processing technique for Lamb wave SHM enabling the identification of mode reflections related to the plate boundaries, and assess their contribution to damage characterisation. The objectives are to: (1) identify propagation paths followed by the waves reflected from the edges and received by the sensors; (2) enable image reconstruction of plate boundaries; (3) assess how the waveform, and especially the wave packets related to edge reflection, are affected by defects (4) identify damage-induced reflections to assist the characterisation of damage within the entire component. The experimental procedure requires the collection of A-scans in a pitch-catch configuration from a circular array of sixteen piezoelectric disk transducers (acting as either sensor or actuator) bonded to an aluminium plate. A tone burst signal tuned for the fundamental symmetric mode (S0) is transmitted and the resulting signals are processed with MATLAB to obtain the distance travelled by each wave packet. The reflected propagation paths can then be determined based on the distance travelled, the transmitter and sensor location, and the theoretical reflection behaviour. The contribution of the different paths to the waveform is experimentally assessed by introducing coupling defects and observing the changes they induced on the wave packets. Features of the plate edges, and waveform reflections are characterised resulting in a significantly larger inspected region.

1 INTRODUCTION

Considerable research has shown that structural health monitoring (SHM) methods based on Lamb wave (guided wave) sensing enables damage detection in metal and composite structures. This sensing technique requires the generation of guided waves using piezoelectric wafer active sensors (PWAS) bonded on the material surface (or embedded in the case of composites) and subsequent observation of these waves propagating throughout a structure. The waveform of the received signal, displayed in amplitude vs time graph (A-scan), contains information on the guided wave modes relating to the propagation medium, including any damage. This in-situ and on-demand inspection method shows particular promise for improving the maintenance of aircraft structures. Advantages include its relatively large area of inspection, non-invasive implementation and moderate cost. However,

there is complexity in interpreting the A-scans from multiple sensors when attempting to locate and characterise defects. Additionally, existing post-processing methods only include the time of flight (ToF) analysis for the direct paths between multiple sensors. Through using reflected signals from free edges, a potentially considerable extension of the field of view is possible. Characterising the reflection paths also allows for the identification of extrinsic features (such as the relative location and orientation of plate boundaries), improving the accuracy of damage location across the structure.

In this study, a post-processing method is proposed utilising a network of multiple PWAS bounded to a square aluminium plate. After an actuation frequency is selected, the sensors are located via triangulation in the time domain, the first reflections are empirically characterised to locate plate boundaries (again, in the time domain), and the plate dimensions are input to convert the relative locations of sensors and plate boundaries from the time domain to the spatial domain. From this, the wave speed and location of sensors are computed, and a comparison of the computed baseline locations with the experimental setup serves as verification for the post-processing technique, and validation of the empirical assumptions regarding the reflected paths. Knowledge of the reflected behaviour for the baseline signal is then used to observe a simulated defect outside of the array of sensors, in addition to identifying a 10mm diameter hole within the array of sensors due to the presence of new reflection.

2 LAMB WAVES

2.1 Lamb Wave testing with PWAS

Lamb waves, also known as guided waves, are a type of dispersive, ultrasonic waves propagating in thin plates [1, 2]. Different modes can exist simultaneously at any given frequency. The two most common type of modes are symmetric (designated S0, S1, …, Sn) and antisymmetric (designated A0, A1, …, An). The symmetric modes have an in-plane particle motion in the same direction as the wave propagation direction, while the antisymmetric modes have an out of plane particle motion, and hence travel perpendicular to the wave propagation direction [2]. Both symmetric and antisymmetric modes propagate through the whole plate thickness.

Their interaction with defects in the structure can affect their propagation and, hence, modify their received signal's waveform. Changes in the waveform can be evaluated by comparing the signal obtained for each assessment with a baseline signal (representative of an undamaged state) [3]. Common changes observed in the waveform include: delay in the arrival time (ToF) of a mode [4], local attenuation [5], presence of new reflection, or mode conversion phenomenon [6, 7]. Several investigations observed that in order to detect damage the signal wavelength has to be smaller than the damage size [2, 4, 5].

Piezoelectric wafer active sensors (PWAS), consisting of lead zirconate titanate (PZT), can be used for both the transmission and sensing of Lamb wave signals. This enables the use of PWAS in different configurations, such as pulse-echo (waves generated and received with the same transducer) or pitch and catch (separate emitter and receiver transducer) [8].

2.2 Lamb Wave Reflections

In some cases the interaction of normal incident Lamb waves with damage was found to lead to mode conversion for the reflected waves. For instance, Willberg et al. [6] observed the conversion of a fundamental symmetric mode (S0) into a fundamental antisymmetric mode (A0) due to a circular defect in a carbon fibre reinforced polymer composite.

Shantanam and Demirli [9] investigated how obliquely incident Lamb waves are reflected at the boundaries of an aluminium plate for different excitation frequencies. They found that for both, A0- and S0- mode, obliquely incident angles (between 0° and 90°) produced multiple mode reflections. The reflection of an incident A0 was partitioned between A0, A1 and SH1 (shear waves), while S0 was partitioned between S0 and SH0. Part of the energy of the incident mode was distributed between the reflected modes. Amongst the reflected modes, A0 was not always found to exhibit the highest energy when the incident waves were A0 and was, therefore, difficult to detect. However the incident S0 mode tended to exhibit detectable S0 reflection for all range of angles, reflecting at the same angle as the incident waves.

2.3 Damage imaging based on sum and delay beamforming

Several attempts have been made to develop an ultrasonic imaging system based on guided waves for metal or composite materials either for non-destructive inspection or SHM. Some of the techniques investigated involve post processing in the time domain including triangulation or sum and delay beamforming [10, 11]. The delay and sum beamforming (DAS) originate from the Synthetic Aperture Focusing Technique (SAFT).

SAFT is a signal processing method that combines an ultrasonic signal's waveforms (recorded at different locations using moving sensor) through a process of summation and time shifting that takes into account waves' velocities and path across the volume [12]. Extensive literature describes the uses of SAFT to investigate concrete structures [13-15] and metal, including aluminium [16, 17] or steel pipes [18, 19]. It results in an enhanced signal to noise ratio and resolution. However it requires accurate knowledge of the wave speed and the sensor position.

Several researchers attempted to use a modified SAFT or DAS for ultrasonic imaging of aluminium and composites plate using guided waves signals. This technique was adapted to accommodate array of static sensors such as found in SHM application. Some investigations included data collected in pulse echo configuration [20], then the technique was adapted to accommodate pitch and catch configuration [21, 22]. Finally, the evolution of SAFT equation gave rise to the Total Focusing Method (TFM). TFM enable image reconstruction for array with multiple emitter and receiver [10, 19].

In most cases the multiple reflections from the plate boundaries are considered as noise to the image reconstruction due to superimposition with the reflection from the damage or generation of artefacts [23]. To avoid this issue some researchers constrained their investigation to the direct path, within an array of sensors. Consequently, the assessed region is limited to within the array of sensors. Alternatively, another method consists of subtracting the test data from a baseline to enhance the changes in the waveform due to damage [11]. However, the use of baseline data prevents the detection of inherent defects.

3 EXPERIMENT

3.1 Materials and sensor positioning

The material investigated is an aluminium plate of 1m × 1m × 2mm, of the following type: AW 1050A–H14 (provided by Smith Metal). The PZT transducers used for this investigation are 0.5 mm thick and 10 mm diameter piezoelectric ceramic disks (supplied by PI ceramic), with a frequency coefficient (N_p) of 2000 Hz.m^{-1}, a mechanical quality factor (Q) of 80 and resonance frequency (f_s) of 200 kHz. A set of 16 piezoelectric disks were bonded to the plate surface. The array's position and the labelling of the PZT sensors are illustrated in Figure 1.

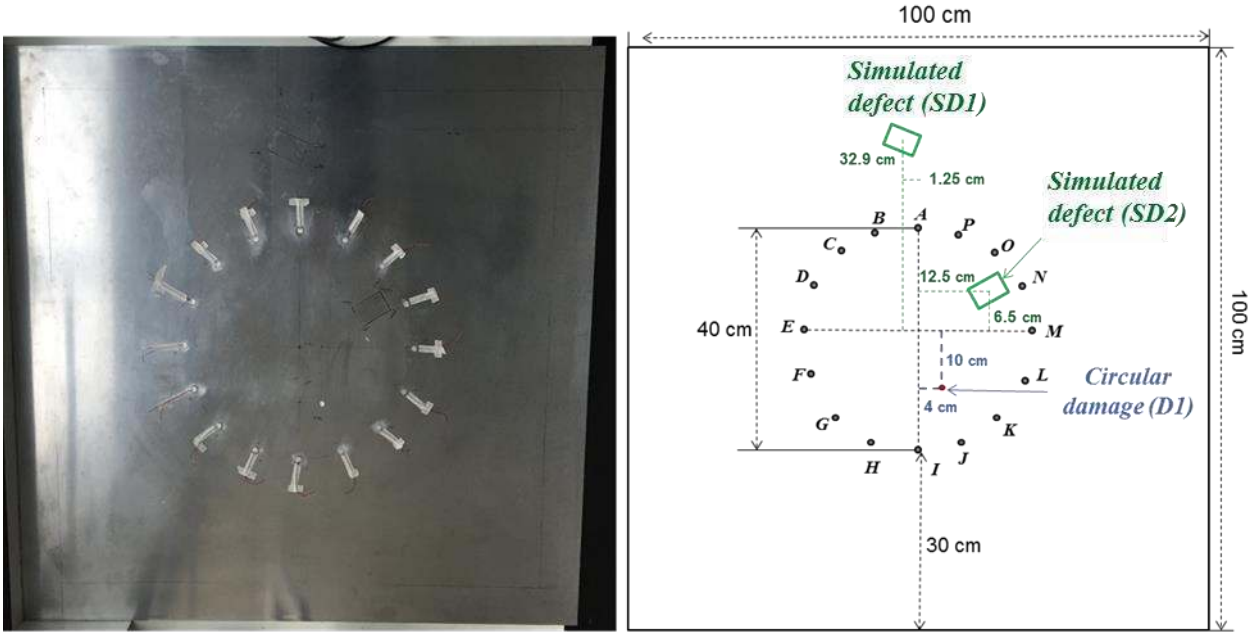

Figure 1: Picture (left) and schematic (right) of the aluminium plate (of dimension 1m× 1m× 0.002m) showing the position of the sensors (10 mm diameter and 0.5 mm thick), the location were the simulated defects were generated (by coupling effect) and the position were the real damage (circular hole of 10mm diameter) was inserted.

3.2 Equipment and Instrumentation

All data were collected in pitch and catch configuration. A signal generator (model: Arbitrary/Function Generator AFG3052C, from Tektronix) was used to generate a three cycle tone burst signal of 10V amplitude to each PZT transducer acting as transmitter. The PZT transducers acting as sensors were connected to an oscilloscope (model: Digital Phosphor Oscilloscope DPO5034B, from Tektronix). The oscilloscope was used to record both the excitation signal generated by the transmitter and the signal response from the sensors. The signals were recorded at a sample rate of 200MHz and each recorded signal was an average of 1000 successive A-scans.

3.3 Experimental procedure

A series of response signals were obtained by varying the frequency of the excitation signal from 30 kHz to 600 kHz. The resulting dispersion and tuning curves are shown in Figure 2 and Figure 3. The procedure to obtain the experimental dispersion and tuning curve can be described as follows: (1) the Hilbert transform of the input and output signal was derived; (2) a low pass filter was implemented to smooth the data; (3) the time of flight was calculated by subtracting the time of the maximum amplitude of the received signal from the time of the maximum amplitude of the transmitted signal; (4) The group velocity was then obtained by dividing the distance between the sensors (40 cm) with the time of flight.

The theoretical data were obtained using the program "WaveFromRevealer 1.0" (from LAMSS© 2011) [24]. The comparison between the experimental and the theoretical data enabled the identification of the modes present in the waveform of each signal.

It can be observed on the tuning curves in Figure 3 that S0 mode is tuned at 300 kHz, which reduces the dispersion effect at this frequency. Therefore this frequency was used for the subsequent data collection (ie: Baseline, Test 1 and Test 2).

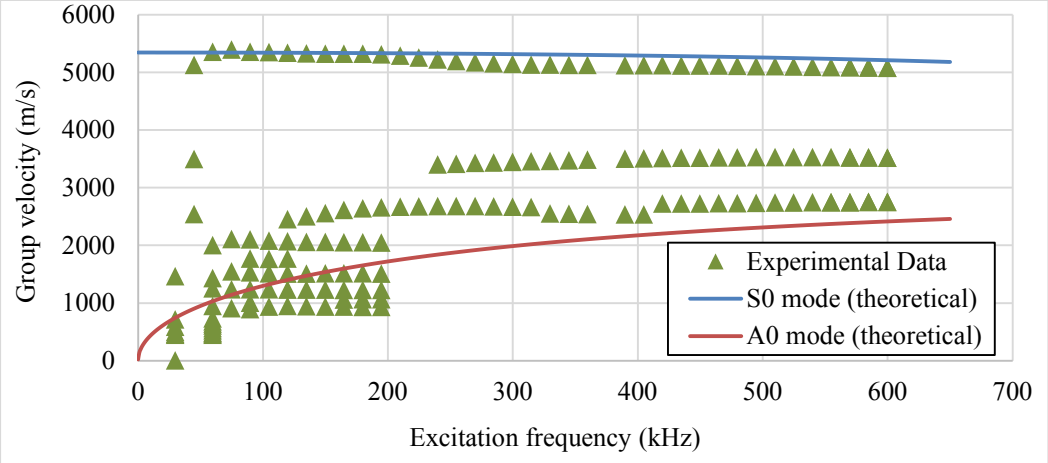

Figure 2: Dispersion curves of the aluminium plate.

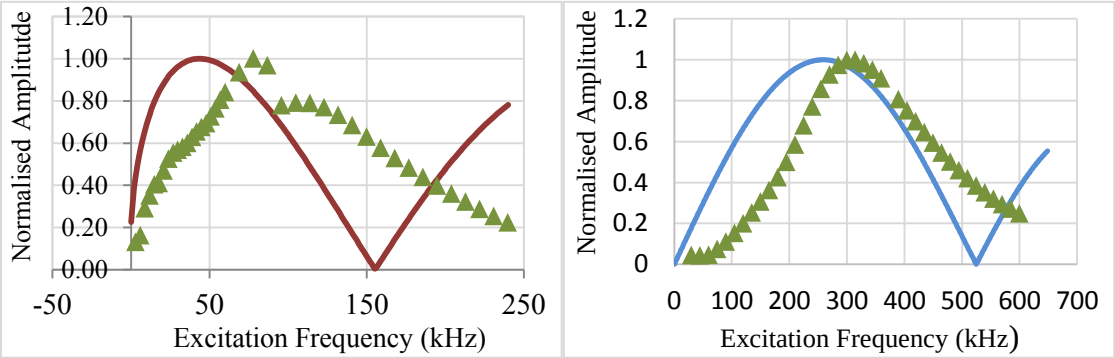

Figure 3: Tuning curve of the antisymmetric mode in red (left) and the symmetric mode in blue (right); the theoretical data (represented in green).

Once the operating frequency was selected, the baseline signals were collected, providing 240 signals with each transducer successively as emitter or receiver.

In the first investigation, Test 1, data were collected with the presence of a circular damage. A circular hole (D1) of 10 mm diameter was drilled in the aluminium plate, the location of the defect is shown in Figure 1. A second experimental investigation was performed, consisting of two coupling defects, SD1 and SD2, in the two locations such as shown in Figure 1 (right). Coupling was achieved using an ultrasonic gel and two rectangular metallic blocks. The detail of the defect size and related data can be found in Table 1.

Data name:	Defect type:	Defect denomination:	Defect dimensions:
Baseline	n/a	n/a	n/a
Test 1	Circular hole	D1	10 mm diameter
Test 2	Surface coupling with block 1	SD1	Area 59 mm× 38 mm (759g)
Test 2	Surface coupling with block 2	SD2	Area: 54 mm× 37mm (730g)

Table 1: Summary and description of the different defects contained the three series of data collected (Baseline, Test 1 and Test 2), the location of each defect can be found Figure 1.

4 POST PROCESSING OF THE BASELINE SIGNAL

4.1 Sensor positioning in time domain

The location of the sensors on the plate surface as well as the location of the free edges of the plate was determined using the baseline signals. Considering that the signals are tuned on

S0 mode and that the PZT emitter generates a circular wave source, each waveform of the received signal can be divided into different sections. The first wave packet corresponds to the propagation of S0 mode on the direct path from the transmitter to the receiver transducer; while the subsequent wave packets are the reflected waves of S0 mode at the plate boundaries.

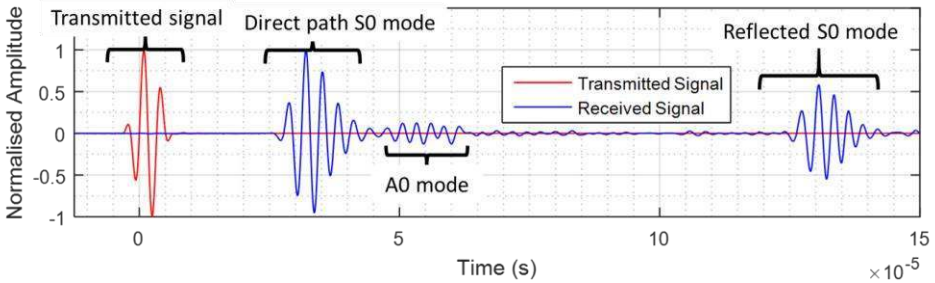

Figure 4: Example of transmitted and received baseline signal at 300kHz showing a tuned S0 mode, attenuated A0 mode, the first edge reflection of S0.

Therefore the time of flight of each wave packet is proportional to the distance travelled by each mode or reflection. The positions of the transducers were found by triangulation of the time of flight of S0 mode (first wave packet).

4.2 Error analysis

In order to verify the calculation of time of flight for this experimental setup, the time of flight between any two transducers was compared with the return path for the baseline signal. The direct percentage error was calculated using Equation (1):

$$\text{Error} = 100 \times \left(\frac{t_{AB} - t_{BA}}{0.5 \times (t_{AB} + t_{BA})} \right) \tag{1}$$

The percentage error between the transducers is plotted in Figure 5. Note that the absence of any clear pattern, which would indicate a systematic error, in addition to the low magnitude (maximum error is below 0.5%) verify the validity of the experimental results. The error distribution presented is assumed to be randomly distributed, and within acceptable limits.

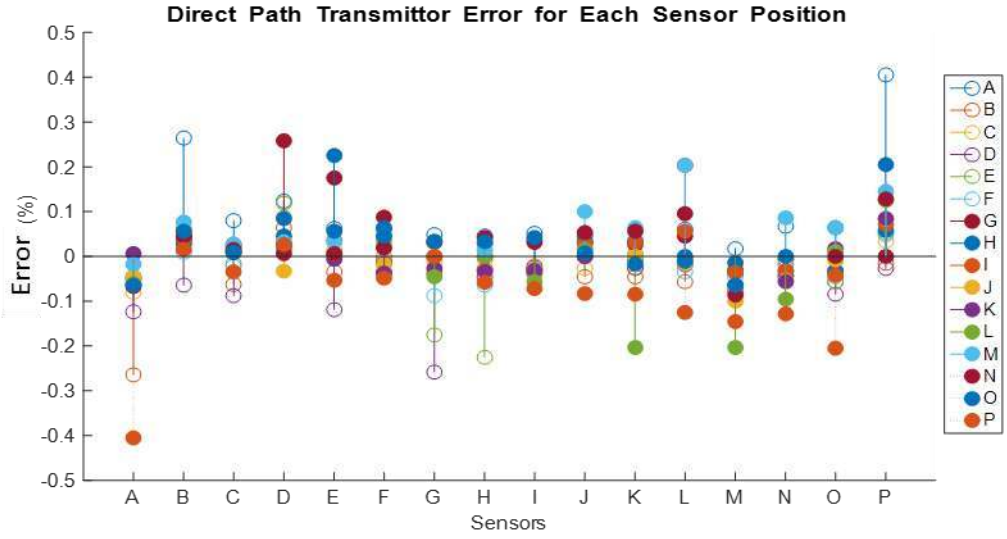

Figure 5: Direct path transmitter percentage error distribution for each sensor position.

4.3 Edge detection, transition to spatial domain and wave speed determination

The position of the plate boundaries relative to the transducers was determined using the time of flight of the second wave packet, which is assumed to be a single reflection from an edge. It was assumed (based on previous literature [9]) that when S0 mode hit the free edge of the plate it was reflected with the same angle, and at the same speed, as the incident waves. Whilst past literature has shown this is not always the case, such a solution can provide the position and angle of the edge with respect to the transmitter and receiver. In combining multiple, separate transmitter/receiver signals, it is possible to construct edge boundaries using only the predicted reflections which are in agreement, and ignoring isolated solutions. Following this assumption, all possible solutions representing where the reflection could occur can be described by an ellipse (assuming only one reflection occurred on the wave's path). The two foci of this ellipse are the emitter and receiver transducers, the time of flight for the first wave packet represents the distance between the two foci (Path 1 in Figure 6), and the reflected distance is represented by the time of flight for the reflected wave packet (Path 2 in Figure 6). The tangent to the ellipse at any point represents the edge angle necessary for a specular reflection at that point.

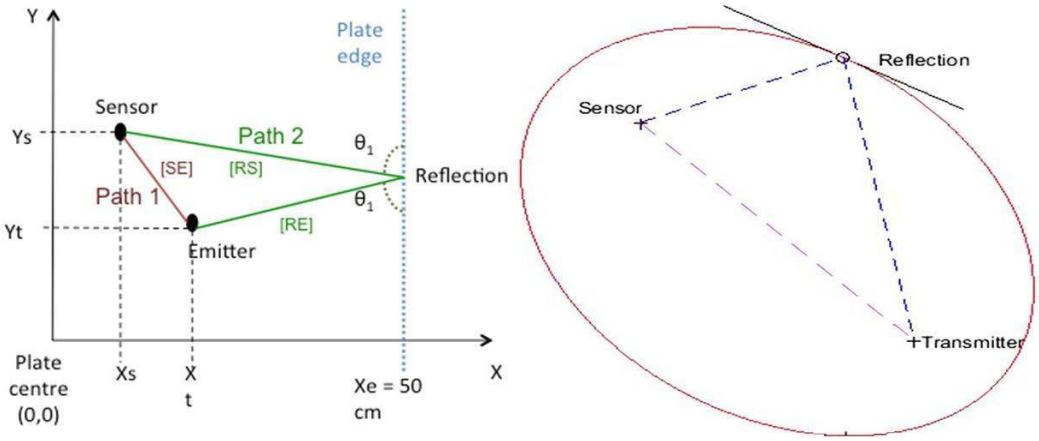

Figure 6: Example of the direct path (path 1) and first reflected path (path 2) from the closest edge (left) and an example of an ellipse with the possible location of the closest edge (in red) (right).

Two ellipses, constructed from two different transducer combinations, would have two common tangents. These common tangents represent an isolated solution. Where more ellipses also share a common tangent with the first two ellipses, the common tangent is considered to be the plate boundary. An example of this is shown in Figure 7, where all isolated solutions are shown as black, dotted lines, and the plate boundary, shared by more than two ellipses is shown as a blue line. In this example, only the reflections produced when the transducer 'A' acts as the transmitter are considered. It is also worth noting that Figure 7 is plotted in the time domain and the triangulated locations of all other transducers are also plotted (with 'A' as the reference).

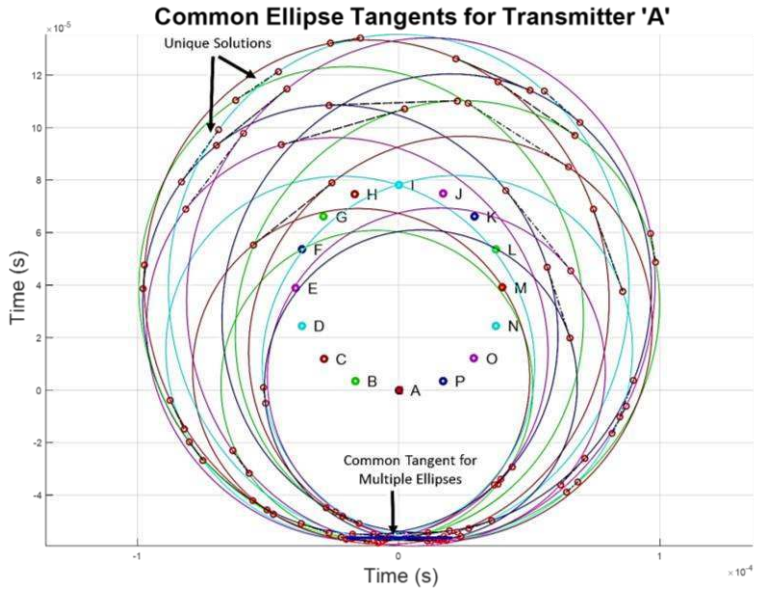

Figure 7: Representation of the detection of the edge location using common ellipse solution (in the time domain).

A common tangent is calculated by comparing the angle and y-intercept of an ellipse tangent with another ellipse tangent. If the magnitude of the difference of both is less than 1% then the tangents are considered common. The 1% error value is calculated from the error anlysis in the previous section where the maximum post-processing error for a single transducer combination is 0.5%, since two are required to form a comparison, the maximum permissable error is assumed as 1%.

Applying this method to all transducer combinations produces the ellipses shown in Figure 8. From this, four clear boundaries are observed. Applying the knowledge that the plate is a 1m x 1m square enables the coordinate conversion from the time domain to the space domain. Figure ojiopj shows the calculated transducer position in the space domain (blue) compared to the assumed transducer position (red).

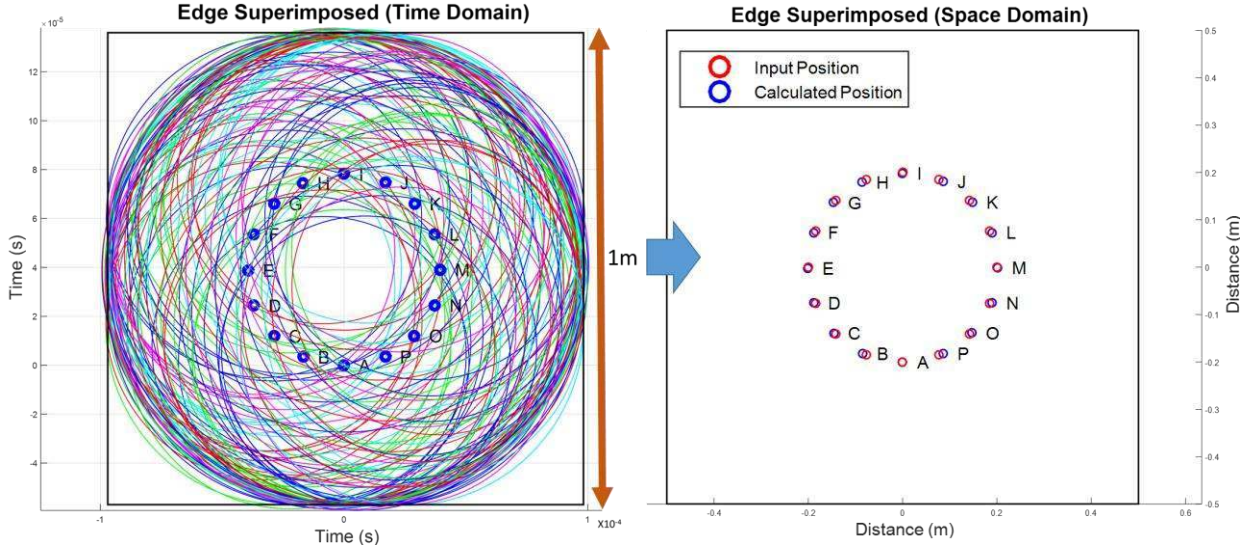

Figure 8: Representation in the time domain of all ellipses derived from the 240 baseline signal (right) and comparison between the input (or measured) sensors position with the position calculated with the post processing of the signal.

Following the conversion to the space domain, the wave speed can also be calculated using Equation 1, substituting the distance travelled and time as the plate dimensions in the space and time domain respectively.

$$\text{Wave Speed} = \frac{distance\ travelled}{time} = \frac{1}{0.00019527} = 5121.1 m.s^{-1} \quad (1)$$

The wave speed of 5121.1 m.s^{-1} compares favourably with the wave speed calculated from the S0 mode tuning curve in Figure 3. As a consequence of this, the assumed path of the reflected wave packets can be considered accurate for the transducer combinations which share multiple common tangents. These wave paths are shown in Figure 9 (in red), alongside the direct paths (in black). This represents a significant extension to the area of inspection.

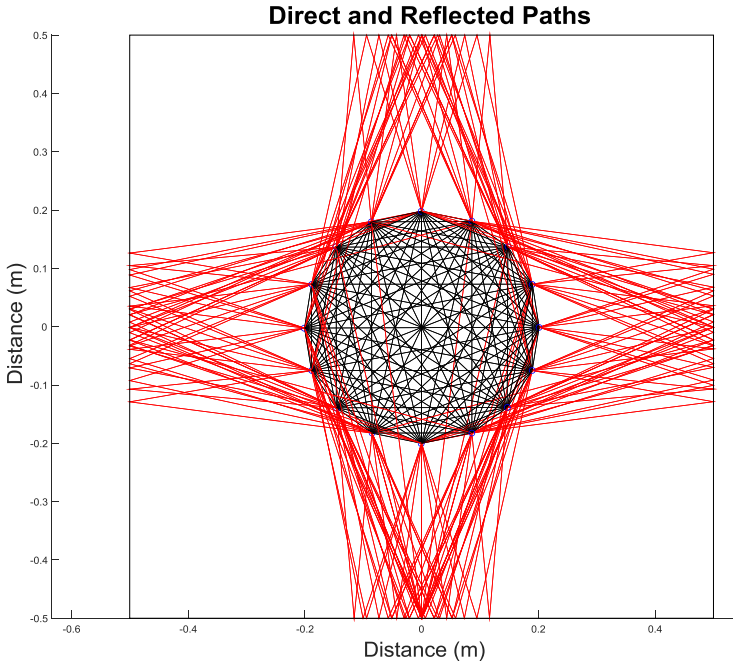

Figure 9: Representation in the special domain of the direct wave's paths (in black) and the reflected wave's paths validated with common tangents (in red).

Following the processing of the baseline signal, it is possible to inspect both the direct, and reflected S0 signal in order to observe damage from the simulated damage in Test 2, in addition to looking for new, specular reflections in the circular damage for Test 1.

5 RESULTS

5.1 Circular damage (Test 1)

For the circular damage, the A-Scan from all sensors for transmitter, 'I', is shown in Figure 1. Despite the damage being smaller than is usually identifiable as the signal wavelength is 1.7cm and the diameter of the hole is 1.0cm, the damage is evidenced by attenuation of the first wave packet on the I-N signal (upper right of Figure 10). In addition to this, a specular reflection was observed. The black circles plotted on the A-Scan in Figure 10 show where a specular reflection from the damage is expected to occur, based on the ellipse theory. On the I-J and I-H signals, a reflection is clearly observed where expected (lower right of Figure 10). Consequently, identifying specular reflections which are not present on the baseline can also be used to identify and locate damage.

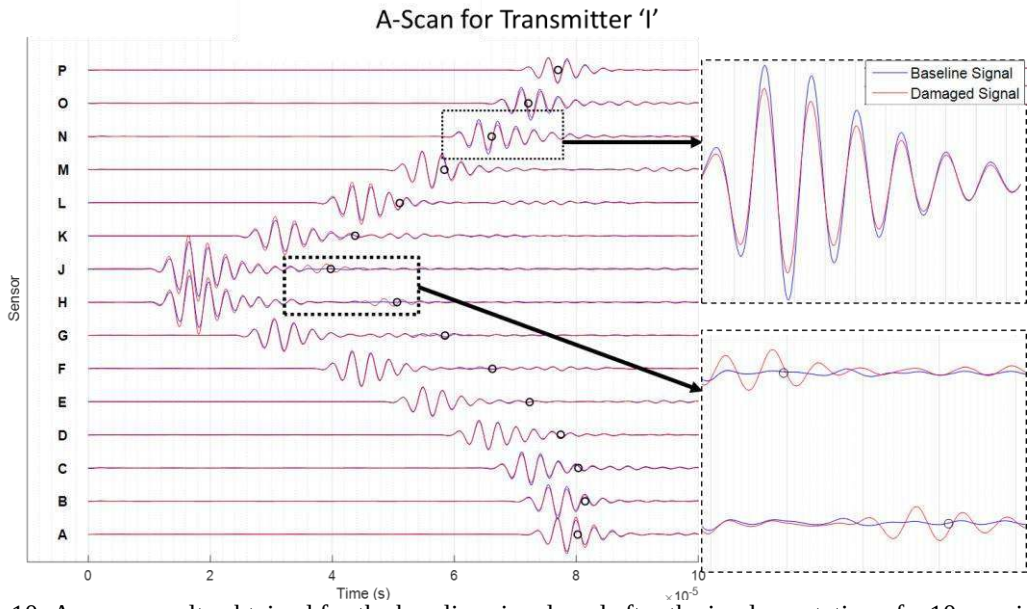

Figure 10: A-scans results obtained for the baseline signal, and after the implementation of a 10mm circular hole, when transducer 'I' is transmitting.

5.1 Simulated damage by coupling (Test 2)

For Test 2, simulated damage was applied as in Figure 1. Figure 11 shows the amplitude vs time graph (A-Scan) from all other sensors with the transducer, 'A', acting as transmitter. The A-Scan shows the simulated damage signal (red), and the baseline signal (blue). The damaged signals for A-N, A-M and A-L are clearly attenuated when compared to the baseline (upper right of Figure 11). The simulated damage, SD2, lies on the direct path travelled by those signals, indicated that the attenuation is caused by SD2. Interestingly, the signal A-I shows similar attenuation on the second wave packet, representing the reflected signal (lower right of Figure 11), but no attenuation on the first wave packet, representing the direct path. This is clear evidence of the simulated damage, SD1, strongly suggesting that reflected signals can be used to identify and locate damage in the same way as direct signals.

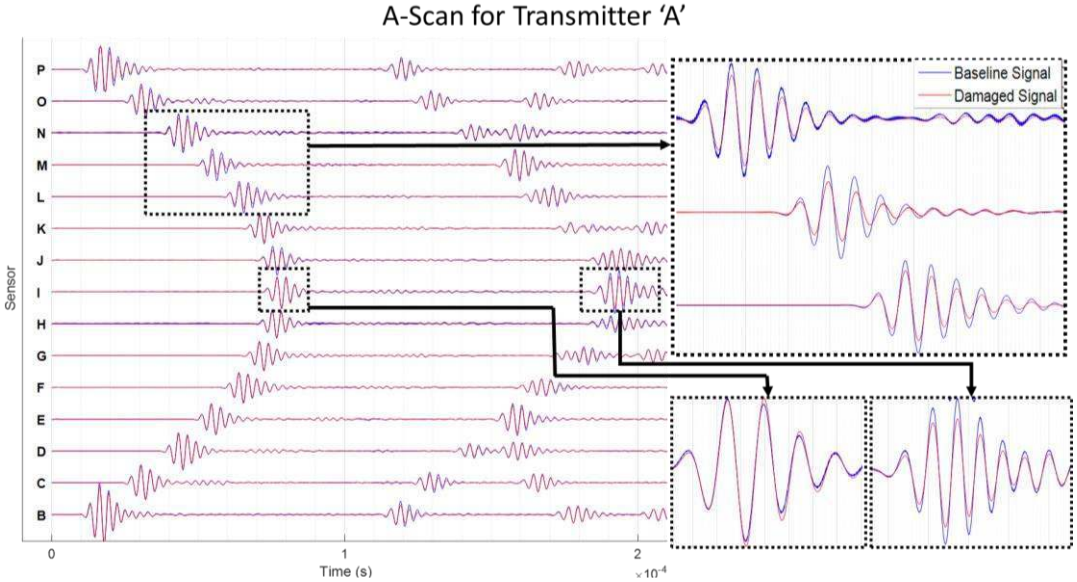

Figure 11: A-scans results obtained for the baseline signal, and after the implementation two coupling defects, when transducer 'A' is transmitting.

6 CONCLUSIONS AND FUTURE WORK

This paper proposed a post processing method of guided wave signals (tuned on S0 mode) obtained in pitch and catch configuration with a circular array of 16 PZT sensors. The relative position between sensors and the plate boundaries was calculated using the baseline signal in the time domain. To do so, it was assumed that the waves hitting the plate boundary were reflected with the same angle as the angle of the incident waves. Therefore the possible edge location could be defined by finding common tangents between the ellipses defined by the time of flight of the reflected waves (their foci being the related transmitter and receiver of the signal analysed). This post processing prevented the propagation of errors due to input measurements, instead the plate size was the only measured value implemented to transit from the time to the space domain. Based on this, the wave speed was recalculated and found to be 5121 $m.s^{-1}$ with a signal wavelength of 17mm.The error due to the processing of the time of flight was found to be less than 0.5%. The post processing of the baseline also served to validate reflected wave paths.

Two experiments were performed with different defects. The comparison of the baseline with the data from the circular damage enabled to identify the presence of local attenuation and a new wave packet (associated with the reflection form damage) in the A –scan. Further processing could enable the characterisation of defects despite the defect size being smaller than the resolution of the waves.

The analysis of the data containing coupling defects, compared with the baseline, showed local attenuation in waves travelling on the direct path, and in waves reflected from the edge. Further processing could enable the defect to be characterised. The use of the information provided by the reflected waves would also enable the region of inspection to be substantially extended.

Future work will include the subtraction of the baseline signal to the test data and development of modified SAFT to locate and quantify the damage. This processing will also focus on incorporating the information provided by the waves reflected from the boundaries of the plate.

ACKNOWLEDGEMENT

This research was supported by the Aerospace Research Institute of the University of Manchester.

REFERENCES

[1] V. Giurgiutiu, "*Structural Health Monitoring with Piezoelectric Wafer Active Sensors"*. Elsevier Inc., IBSN-13: 978-0-12-088760-6 (2008)

[2] Z. Su and L. Ye, "*Identification of Damage Using Lamb waves From Fundamentals to Applications"*. F. Pfeiffer, P. Wriggers (Eds), vol.48, ISBN: 978-1-84882-783-7 (2009)

[3] J. B. Ihn and F. K. Chang, Detection and monitoring of hidden fatigue crack growth using a built-in piezoelectric sensor / actuator network : I . Diagnostics. Smart Materials and Structures, 13, 609-620, 2004.

[4] K. Diamanti and C. Soutis, Structural health monitoring techniques for aircraft composite structures. Progress in Aerospace Sciences, 46(8), 342-352, 2010.

[5] S. Grondel, J. Assaad, C. Delebarre and E. Moulin, Health monitoring of a composite wingbox structure. Ultrasonics, 42(1-9), 814-824, 2004.

[6] C. Willberg, S. Koch, G. Mook, J. Pohl and U. Gabbert, Continuous mode conversion of Lamb waves in CFRP plates. Smart Materials and Structures,21, 2012.

[7] W. J. Staszweski, S. Mahzan and R. Traynor, Health monitoring of aerospace composite structures – Active and

passive approach. Composites Science and Technology, 69(11-12), 1678–1685, 2008.

[8] M. Gresil and V. Giurgiutiu, Prediction of attenuated guided waves propagation in carbon fiber composites using Rayleigh damping model. Journal of Intelligent Materials Systems and Structures, 26(16), 2015.

[9] S. Santhanam and R. Demirli, Reflection of Lamb waves obliquely incident on the free edge of a plate. Ultrasonics, 53, 271-282, 2012.

[10] C. Fan, M. Caleap, M. Pan and B. W. Drinkwater, A comparison between ultrasonic array beamforming and super resolution imaging algorithms for non-destructive evaluation. Ultrasonics, 54, 1842-1850, 2014.

[11] G. Giridhara, V. T. Rathod, S. Naik, D. Roy Mahapatra and S. Gopalakrishnan, Rapid localization of damage using circular sensor array and Lamb wave based triangulation. Mechanical Systems and Signal Processing, 24, 2929-2946, 2010.

[12] S. Kramer, Ultrasonic weld defect sizing using the synthetic aperture focusing technique. Review of Progress in Quantitative Nondestructive Evaluation, 8(9), 1995-2002, IBSN: 978-1-4612-8097-2 (1989).

[13] P. A. Gaydecki , F. M. Burdekin, W. Damaj, D. G. John and P. A. Payne, Digital deconvolution analysis of ultrasonic influenced by the presence of longitudinally aligned steel cables in pre-stressed concrete. Measurement Science and Technology, 3(9), 909-917, 1992.

[14] H. T. Shandiz and P. A. Gaydecki, An enhanced, high-speed ultrasonic SAFT system for imaging of defects within concrete structures. American Institute of Physics conference proceedings 557, 703, 2001.

[15] M. Schikert, M. Krause and W. Muller, Ultrasonic Imaging of Concrete Elements Using Reconstruction by Synthetic Aperture Focusing Technique. Journal of Materials in Civil Engineering, 5(3), 235-246, 2003.

[16] R. N. Thomson , Transverse and longitudinal resolution of the synthetic aperture focusing technique. Ultrasonics, 22(1), 9-15, 1984.

[17] W. M. Masri "Diffraction-corrected synthetic aperture focusing for spherical ultrasonic radiators ". Retrospective Theses and Dissertations, Iowa State University, USA, 1997.

[18] T. Gaul, L. Schubert, B. Weihnacht and B. Frankenstein, Localization of Defects in Pipes Using Guided Waves and Synthetic Aperture Focussing Technique (SAFT). Proceedings of the 7th European Workshop on Structural Health Monitoring, Nantes, France, 2014.

[19] T. Stepinski, L. Ambrozinski, and T. Uhl , Beamforming of Lamb waves using 2D arrays: A comparative study. Structural Health Monitoring 2013, ed. Fu-Kuo Chang, Proceedings of the 9th International Workshop on SHM Stanford University, Stanford, USA, 2210-2217, 2013.

[20] L. Yu and V. Giurgiutiu, Improvement of Damage Detection with the Embedded Ultrasonics Structural Radar for Structural Heath Monitoring. Proceedings of 5th International Workshop on Structural Health Monitoring, Stanford University, Stanford, USA, 2005.

[21] C. J. Lissenden and J. L. Rose, Structural Health Monitoring of Composite laminates Through Ultrasonic Guided Wave Beam Forming. Proceedings of NATO Applied Vehicle Technology Symposium on Military Platform, RTO-MP-AVT-157, 2014.

[22] F. Li, H. Peng and G. Meng, Quantitative damage image construction in plate structures using a circular PZT array and Lamb waves. Sensors and Actuators, A, 214, 66-73, 2014.

[23] J. S. Hall and J. E. Michael, Multipath ultrasonic guided wave imaging in complex structures. Structural Health Monitoring, 14(4), 345-358, 2015.

[24] Y., Shen and V. Giurgiutiu, WaveFormRevealer: An analytical framework and predictive tool for the simulation of multi-modal guided wave propagation and interaction with damage. Structural Health Monitoring – An International Journal, 13(5), 491-511, doi: 10.1177/1475921714532986 (2014).